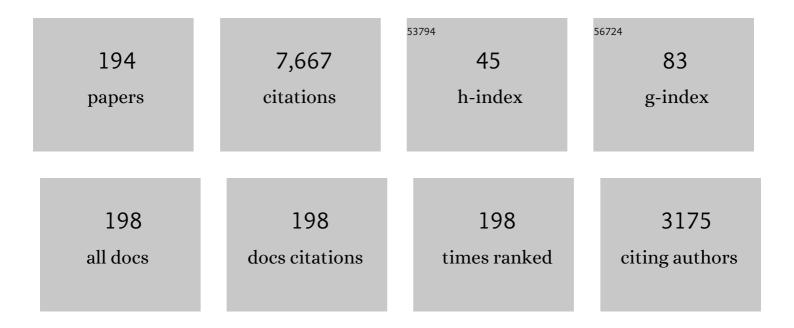
## Vania Da Deppo

List of Publications by Year in descending order

Source: https://exaly.com/author-pdf/609648/publications.pdf Version: 2024-02-01



**ΝΑΝΙΑ ΠΑ ΠΕΡΡΟ** 

#	Article	IF	CITATIONS
1	On the nucleus structure and activity of comet 67P/Churyumov-Gerasimenko. Science, 2015, 347, aaa1044.	12.6	366
2	Dust measurements in the coma of comet 67P/Churyumov-Gerasimenko inbound to the Sun. Science, 2015, 347, aaa3905.	12.6	310
3	OSIRIS – The Scientific Camera System Onboard Rosetta. Space Science Reviews, 2007, 128, 433-506.	8.1	286
4	The morphological diversity of comet 67P/Churyumov-Gerasimenko. Science, 2015, 347, aaa0440.	12.6	259
5	The global shape, density and rotation of Comet 67P/Churyumov-Gerasimenko from preperihelion Rosetta/OSIRIS observations. Icarus, 2016, 277, 257-278.	2.5	252
6	Shape model, reference system definition, and cartographic mapping standards for comet 67P/Churyumov-Gerasimenko – Stereo-photogrammetric analysis of Rosetta/OSIRIS image data. Astronomy and Astrophysics, 2015, 583, A33.	5.1	188
7	Spectrophotometric properties of the nucleus of comet 67P/Churyumov-Gerasimenko from the OSIRIS instrument onboard the ROSETTA spacecraft. Astronomy and Astrophysics, 2015, 583, A30.	5.1	188
8	Images of Asteroid 21 Lutetia: A Remnant Planetesimal from the Early Solar System. Science, 2011, 334, 487-490.	12.6	179
9	Insolation, erosion, and morphology of comet 67P/Churyumov-Gerasimenko. Astronomy and Astrophysics, 2015, 583, A34.	5.1	173
10	Feasibility of satellite quantum key distribution. New Journal of Physics, 2009, 11, 045017.	2.9	171
11	The primordial nucleus of comet 67P/Churyumov-Gerasimenko. Astronomy and Astrophysics, 2016, 592, A63.	5.1	159
12	Large heterogeneities in comet 67P as revealed by active pits from sinkhole collapse. Nature, 2015, 523, 63-66.	27.8	158
13	EVOLUTION OF THE DUST SIZE DISTRIBUTION OF COMET 67P/CHURYUMOV–GERASIMENKO FROM 2.2 au TO PERIHELION. Astrophysical Journal, 2016, 821, 19.	4.5	158
14	Regional surface morphology of comet 67P/Churyumov-Gerasimenko from Rosetta/OSIRIS images. Astronomy and Astrophysics, 2015, 583, A26.	5.1	153
15	Redistribution of particles across the nucleus of comet 67P/Churyumov-Gerasimenko. Astronomy and Astrophysics, 2015, 583, A17.	5.1	149
16	Two independent and primitive envelopes of the bilobate nucleus of comet 67P. Nature, 2015, 526, 402-405.	27.8	141
17	E-Type Asteroid (2867) Steins as Imaged by OSIRIS on Board Rosetta. Science, 2010, 327, 190-193.	12.6	120
18	Metis: the Solar Orbiter visible light and ultraviolet coronal imager. Astronomy and Astrophysics, 2020, 642, A10.	5.1	115

#	Article	IF	CITATIONS
19	Gravitational slopes, geomorphology, and material strengths of the nucleus of comet 67P/Churyumov-Gerasimenko from OSIRIS observations. Astronomy and Astrophysics, 2015, 583, A32.	5.1	113
20	Summer fireworks on comet 67P. Monthly Notices of the Royal Astronomical Society, 2016, 462, S184-S194.	4.4	112
21	The Colour and Stereo Surface Imaging System (CaSSIS) for the ExoMars Trace Gas Orbiter. Space Science Reviews, 2017, 212, 1897-1944.	8.1	111
22	Seasonal mass transfer on the nucleus of comet 67P/Chuyumov–Gerasimenko. Monthly Notices of the Royal Astronomical Society, 2017, 469, S357-S371.	4.4	111
23	Size-frequency distribution of boulders ≥7 m on comet 67P/Churyumov-Gerasimenko. Astronomy and Astrophysics, 2015, 583, A37.	5.1	108
24	The global meter-level shape model of comet 67P/Churyumov-Gerasimenko. Astronomy and Astrophysics, 2017, 607, L1.	5.1	107
25	Are fractured cliffs the source of cometary dust jets? Insights from OSIRIS/Rosetta at 67P/Churyumov-Gerasimenko. Astronomy and Astrophysics, 2016, 587, A14.	5.1	102
26	The pristine interior of comet 67P revealed by the combined Aswan outburst and cliff collapse. Nature Astronomy, 2017, 1, .	10.1	100
27	OSIRIS observations of meter-sized exposures of H <sub>2</sub> 0 ice at the surface of 67P/Churyumov-Gerasimenko and interpretation using laboratory experiments. Astronomy and Astrophysics, 2015, 583, A25.	5.1	97
28	Rosetta's comet 67P/Churyumov-Gerasimenko sheds its dusty mantle to reveal its icy nature. Science, 2016, 354, 1566-1570.	12.6	97
29	A collision in 2009 as the origin of the debris trail of asteroid P/2010 A2. Nature, 2010, 467, 814-816.	27.8	94
30	Regional surface morphology of comet 67P/Churyumov-Gerasimenko from Rosetta/OSIRIS images: The southern hemisphere. Astronomy and Astrophysics, 2016, 593, A110.	5.1	86
31	The rotation state of 67P/Churyumov-Gerasimenko from approach observations with the OSIRIS cameras on Rosetta. Astronomy and Astrophysics, 2014, 569, L2.	5.1	81
32	Fractures on comet 67P/Churyumovâ€Gerasimenko observed by Rosetta/OSIRIS. Geophysical Research Letters, 2015, 42, 5170-5178.	4.0	71
33	SIMBIO-SYS: The spectrometer and imagers integrated observatory system for the BepiColombo planetary orbiter. Planetary and Space Science, 2010, 58, 125-143.	1.7	70
34	Scientific assessment of the quality of OSIRIS images. Astronomy and Astrophysics, 2015, 583, A46.	5.1	67
35	Detection of exposed H <sub>2</sub> O ice on the nucleus of comet 67P/Churyumov-Gerasimenko. Astronomy and Astrophysics, 2016, 595, A102.	5.1	67
36	Surface changes on comet 67P/Churyumov-Gerasimenko suggest a more active past. Science, 2017, 355, 1392-1395.	12.6	63

#	Article	IF	CITATIONS
37	67P/Churyumov-Gerasimenko: Activity between March and June 2014 as observed from Rosetta/OSIRIS. Astronomy and Astrophysics, 2015, 573, A62.	5.1	60
38	Temporal morphological changes in the Imhotep region of comet 67P/Churyumov-Gerasimenko. Astronomy and Astrophysics, 2015, 583, A36.	5.1	60
39	The 2016 Feb 19 outburst of comet 67P/CG: an ESA Rosetta multi-instrument study. Monthly Notices of the Royal Astronomical Society, 2016, 462, S220-S234.	4.4	60
40	Geomorphology of the Imhotep region on comet 67P/Churyumov-Gerasimenko from OSIRIS observations. Astronomy and Astrophysics, 2015, 583, A35.	5.1	59
41	Sunset jets observed on comet 67P/Churyumov-Gerasimenko sustained by subsurface thermal lag. Astronomy and Astrophysics, 2016, 586, A7.	5.1	55
42	Link budget and background noise for satellite quantum key distribution. Advances in Space Research, 2011, 47, 802-810.	2.6	54
43	Comet 67P/Churyumov-Gerasimenko: Constraints on its origin from OSIRIS observations. Astronomy and Astrophysics, 2015, 583, A44.	5.1	53
44	Aswan site on comet 67P/Churyumov-Gerasimenko: Morphology, boulder evolution, and spectrophotometry. Astronomy and Astrophysics, 2016, 592, A69.	5.1	53
45	Acceleration of individual, decimetre-sized aggregates in the lower coma of comet 67P/Churyumov–Gerasimenko. Monthly Notices of the Royal Astronomical Society, 2016, 462, S78-S88.	4.4	52
46	Evidence of sub-surface energy storage in comet 67P from the outburst of 2016 July 03. Monthly Notices of the Royal Astronomical Society, 2017, 469, s606-s625.	4.4	45
47	The scattering phase function of comet 67P/Churyumov–Gerasimenko coma as seen from the Rosetta/OSIRIS instrument. Monthly Notices of the Royal Astronomical Society, 2017, 469, S404-S415.	4.4	44
48	Seasonal erosion and restoration of the dust cover on comet 67P/Churyumov-Gerasimenko as observed by OSIRIS onboard Rosetta. Astronomy and Astrophysics, 2017, 604, A114.	5.1	43
49	Dust mass distribution around comet 67P/Churyumov–Gerasimenko determined via parallax measurements using Rosetta's OSIRIS cameras. Monthly Notices of the Royal Astronomical Society, 2017, 469, S276-S284.	4.4	43
50	Variegation of comet 67P/Churyumov-Gerasimenko in regions showing activity. Astronomy and Astrophysics, 2016, 586, A80.	5.1	43
51	Iqueye, a single photon-counting photometer applied to the ESO new technology telescope. Astronomy and Astrophysics, 2009, 508, 531-539.	5.1	42
52	Geological map and stratigraphy of asteroid 21 Lutetia. Planetary and Space Science, 2012, 66, 125-136.	1.7	42
53	Geomorphology and spectrophotometry of Philae's landing site on comet 67P/Churyumov-Gerasimenko. Astronomy and Astrophysics, 2015, 583, A41.	5.1	41
54	The pebbles/boulders size distributions on Sais: Rosetta's final landing site on comet 67P/Churyumov–Gerasimenko. Monthly Notices of the Royal Astronomical Society, 2017, 469, S636-S645.	4.4	40

#	Article	IF	CITATIONS
55	Large-scale dust jets in the coma of 67P/Churyumov-Gerasimenko as seen by the OSIRIS instrument onboard Rosetta. Astronomy and Astrophysics, 2015, 583, A9.	5.1	39
56	The dust environment of comet 67P/Churyumov-Gerasimenko from Rosetta OSIRIS and VLT observations in the 4.5 to 2.9 AU heliocentric distance range inbound. Astronomy and Astrophysics, 2016, 587, A155.	5.1	39
57	Thermal modelling of water activity on comet 67P/Churyumov-Gerasimenko with global dust mantle and plural dust-to-ice ratio. Monthly Notices of the Royal Astronomical Society, 2017, 469, S295-S311.	4.4	39
58	CHANGES IN THE PHYSICAL ENVIRONMENT OF THE INNER COMA OF 67P/CHURYUMOV–GERASIMENKO WITH DECREASING HELIOCENTRIC DISTANCE. Astronomical Journal, 2016, 152, 130.	4.7	36
59	AquEYE, a single photon counting photometer for astronomy. Journal of Modern Optics, 2009, 56, 261-272.	1.3	34
60	METIS: a novel coronagraph design for the Solar Orbiter mission. Proceedings of SPIE, 2012, , .	0.8	34
61	Gas outflow and dust transport of comet 67P/Churyumov–Gerasimenko. Monthly Notices of the Royal Astronomical Society, 2016, 462, S533-S546.	4.4	34
62	Observations and analysis of a curved jet in the coma of comet 67P/Churyumov-Gerasimenko. Astronomy and Astrophysics, 2016, 588, L3.	5.1	34
63	Morphology and dynamics of the jets of comet 67P/Churyumov-Gerasimenko: Early-phase development. Astronomy and Astrophysics, 2015, 583, A11.	5.1	33
64	Constraints on cometary surface evolution derived from a statistical analysis of 67P's topography. Monthly Notices of the Royal Astronomical Society, 2017, 469, S329-S338.	4.4	33
65	Meter-scale thermal contraction crack polygons on the nucleus of comet 67P/Churyumov-Gerasimenko. Icarus, 2018, 301, 173-188.	2.5	33
66	Optical design of the single-detector planetary stereo camera for the BepiColombo European Space Agency mission to Mercury. Applied Optics, 2010, 49, 2910.	2.1	32
67	Regional unit definition for the nucleus of comet 67P/Churyumov-Gerasimenko on the SHAP7 model. Planetary and Space Science, 2018, 164, 19-36.	1.7	32
68	(21) Lutetia spectrophotometry from Rosetta-OSIRIS images and comparison to ground-based observations. Planetary and Space Science, 2012, 66, 43-53.	1.7	31
69	The highly active Anhur–Bes regions in the 67P/Churyumov–Gerasimenko comet: results from OSIRIS/ROSETTA observations. Monthly Notices of the Royal Astronomical Society, 2017, 469, S93-S107.	4.4	30
70	Optical design of the multi-wavelength imaging coronagraph Metis for the solar orbiter mission. Experimental Astronomy, 2020, 49, 239-263.	3.7	30
71	A mini outburst from the nightside of comet 67P/Churyumov-Gerasimenko observed by the OSIRIS camera on Rosetta. Astronomy and Astrophysics, 2016, 596, A89.	5.1	29
72	Observations of Comet 9P/Tempel 1 around the Deep Impact event by the OSIRIS cameras onboard Rosetta. Icarus, 2007, 187, 87-103.	2.5	27

#	Article	IF	CITATIONS
73	Geologic mapping of the Comet 67P/Churyumov–Gerasimenko's Northern hemisphere. Monthly Notices of the Royal Astronomical Society, 2016, 462, S352-S367.	4.4	27
74	The southern hemisphere of 67P/Churyumov-Gerasimenko: Analysis of the preperihelion size-frequency distribution of boulders ≥7 m. Astronomy and Astrophysics, 2016, 592, L2.	5.1	27
75	Multi Element Telescope for Imaging and Spectroscopy (METIS) coronagraph for the Solar Orbiter mission. Proceedings of SPIE, 2012, , .	0.8	26
76	Rotating dust particles in the coma of comet 67P/Churyumov-Gerasimenko. Astronomy and Astrophysics, 2015, 583, A14.	5.1	26
77	Characterization of the Abydos region through OSIRIS high-resolution images in support of CIVA measurements. Astronomy and Astrophysics, 2016, 585, L1.	5.1	26
78	Decimetre-scaled spectrophotometric properties of the nucleus of comet 67P/Churyumov–Gerasimenko from OSIRIS observations. Monthly Notices of the Royal Astronomical Society, 2016, 462, S287-S303.	4.4	26
79	Exploring the Solar Wind from Its Source on the Corona into the Inner Heliosphere during the First Solar Orbiter–Parker Solar Probe Quadrature. Astrophysical Journal Letters, 2021, 920, L14.	8.3	25
80	Long-term survival of surface water ice on comet 67P. Monthly Notices of the Royal Astronomical Society, 2017, 469, S582-S597.	4.4	24
81	Method for studying the effects of thermal deformations on optical systems for space application. Applied Optics, 2011, 50, 2836.	2.1	23
82	Orbital elements of the material surrounding comet 67P/Churyumov-Gerasimenko. Astronomy and Astrophysics, 2015, 583, A16.	5.1	23
83	Sublimation of icy aggregates in the coma of comet 67P/Churyumov–Gerasimenko detected with the OSIRIS cameras on board <i>Rosetta</i> . Monthly Notices of the Royal Astronomical Society, 2016, 462, S57-S66.	4.4	23
84	Geomorphological mapping of comet 67P/Churyumov–Gerasimenko's Southern hemisphere. Monthly Notices of the Royal Astronomical Society, 2016, 462, S573-S592.	4.4	23
85	Astronomical applications of quantum optics for extremely large telescopes. Journal of Modern Optics, 2007, 54, 191-197.	1.3	22
86	Physical properties and dynamical relation of the circular depressions on comet 67P/Churyumov-Gerasimenko. Astronomy and Astrophysics, 2016, 591, A132.	5.1	22
87	Bilobate comet morphology and internal structure controlled by shear deformation. Nature Geoscience, 2019, 12, 157-162.	12.9	22
88	On deviations from free-radial outflow in the inner coma of comet 67P/Churyumov–Gerasimenko. Icarus, 2018, 311, 1-22.	2.5	21
89	Spectrophotometry of the Khonsu region on the comet 67P/Churyumov–Gerasimenko using OSIRIS instrument images. Monthly Notices of the Royal Astronomical Society, 2016, 462, S274-S286.	4.4	20
90	The phase function and density of the dust observed at comet 67P/Churyumov–Gerasimenko. Monthly Notices of the Royal Astronomical Society, 2018, 476, 2835-2839.	4.4	20

#	Article	lF	CITATIONS
91	Models of Rosetta/OSIRIS 67P Dust Coma Phase Function. Astronomical Journal, 2018, 156, 237.	4.7	20
92	Coma morphology of comet 67P controlled by insolation over irregular nucleus. Nature Astronomy, 2018, 2, 562-567.	10.1	19
93	Comparative study of water ice exposures on cometary nuclei using multispectral imaging data. Monthly Notices of the Royal Astronomical Society, 2016, 462, S394-S414.	4.4	18
94	CASTAway: An asteroid main belt tour and survey. Advances in Space Research, 2018, 62, 1998-2025.	2.6	18
95	Post-perihelion photometry of dust grains in the coma of 67P Churyumov–Gerasimenko. Monthly Notices of the Royal Astronomical Society, 2017, 469, S195-S203.	4.4	17
96	THE STEREO CAMERA ON THE BEPICOLOMBO ESA/JAXA MISSION: A NOVEL APPROACH. , 2009, , 305-322.		16
97	The Agilkia boulders/pebbles size–frequency distributions: OSIRIS and ROLIS joint observations of 67P surface. Monthly Notices of the Royal Astronomical Society, 2016, 462, S242-S252.	4.4	15
98	Pre-hibernation performances of the OSIRIS cameras onboard the Rosetta spacecraft. Astronomy and Astrophysics, 2015, 574, A123.	5.1	14
99	Possible interpretation of the precession of comet 67P/Churyumov-Gerasimenko. Astronomy and Astrophysics, 2016, 590, A46.	5.1	14
100	QuantEYE, the quantum optics instrument for OWL. Proceedings of the International Astronomical Union, 2005, 1, 506-507.	0.0	13
101	Long-term monitoring of comet 67P/Churyumov–Gerasimenko's jets with OSIRIS onboard Rosetta. Monthly Notices of the Royal Astronomical Society, 2017, 469, S380-S385.	4.4	13
102	Search for satellites near comet 67P/Churyumov-Gerasimenko using Rosetta/OSIRIS images. Astronomy and Astrophysics, 2015, 583, A19.	5.1	13
103	Optical design of the Wide Angle Camera for the Rosetta mission. Applied Optics, 2002, 41, 1446.	2.1	12
104	Observations of Comet 9P/Tempel 1 around the Deep Impact event by the OSIRIS cameras onboard Rosetta. Icarus, 2007, 191, 241-257.	2.5	12
105	Modelling of the outburst on 2015 July 29 observed with OSIRIS cameras in the Southern hemisphere of comet 67P/Churyumov–Gerasimenko. Monthly Notices of the Royal Astronomical Society, 2017, 469, S178-S185.	4.4	12
106	Characterization of dust aggregates in the vicinity of the Rosetta spacecraft. Monthly Notices of the Royal Astronomical Society, 2017, 469, S312-S320.	4.4	12
107	Opposition effect on comet 67P/Churyumov-Gerasimenko using Rosetta-OSIRIS images. Astronomy and Astrophysics, 2017, 599, A11.	5.1	11
108	Multivariate statistical analysis of OSIRIS/Rosetta spectrophotometric data of comet 67P/Churyumov-Gerasimenko. Astronomy and Astrophysics, 2017, 600, A115.	5.1	11

#	Article	IF	CITATIONS
109	Ultraviolet and Visible-light Coronagraphic Imager (UVCI). , 2003, , .		10
110	No wavefront sensor adaptive optics system for compensation of primary aberrations by software analysis of a point source image 1 Methods. Applied Optics, 2007, 46, 6434.	2.1	10
111	Simulations using terrestrial geological analogues to assess interpretability of potential geological features of the Hermean surface restituted by the STereo imaging Camera of the SIMBIOSYS package (BepiColombo mission). Planetary and Space Science, 2008, 56, 1079-1092.	1.7	10
112	Novel space coronagraphs: METIS, a flexible optical design for multi-wavelength imaging and spectroscopy. , 2013, , .		10
113	Photometry of dust grains of comet 67P and connection with nucleus regions. Astronomy and Astrophysics, 2016, 588, A59.	5.1	10
114	On-Ground Performance and Calibration of the ExoMars Trace Gas Orbiter CaSSIS Imager. Space Science Reviews, 2017, 212, 1871-1896.	8.1	10
115	The Rockyâ€Like Behavior of Cometary Landslides on 67P/Churyumovâ€Gerasimenko. Geophysical Research Letters, 2019, 46, 14336-14346.	4.0	9
116	Characterization of OSIRIS NAC filters for the interpretation of multispectral data of comet 67P/Churyumov-Gerasimenko. Astronomy and Astrophysics, 2015, 583, A45.	5.1	8
117	Distance determination method of dust particles using Rosetta OSIRIS NAC and WAC data. Planetary and Space Science, 2017, 143, 256-264.	1.7	8
118	Regional surface morphology of comet 67P/Churyumov-Gerasimenko from Rosetta/OSIRIS images: The southern hemisphere (Corrigendum). Astronomy and Astrophysics, 2017, 598, C2.	5.1	8
119	Geomorphological and spectrophotometric analysis of Seth's circular niches on comet 67P/Churyumov–Gerasimenko using OSIRIS images. Monthly Notices of the Royal Astronomical Society, 2017, 469, S238-S251.	4.4	8
120	Effects of image compression and illumination on digital terrain models for the stereo camera of the BepiColombo mission. Planetary and Space Science, 2017, 136, 1-14.	1.7	8
121	An afocal telescope configuration for the ESA ARIEL mission. CEAS Space Journal, 2017, 9, 379-398.	2.3	8
122	The ARIEL Instrument Control Unit design. Experimental Astronomy, 2018, 46, 1-30.	3.7	8
123	Innovative optical setup for testing a stereo camera for space applications. Proceedings of SPIE, 2012, ,	0.8	7
124	Radiometric model for the stereo camera STC onboard the BepiColombo ESA mission. Proceedings of SPIE, 2016, , .	0.8	7
125	Thermophysics of fractures on comet 67P/Churyumov-Gerasimenko. Astronomy and Astrophysics, 2017, 608, A121.	5.1	7
126	The big lobe of 67P/Churyumov–Gerasimenko comet: morphological and spectrophotometric evidences of layering as from OSIRIS data. Monthly Notices of the Royal Astronomical Society, 2018, 479, 1555-1568.	4.4	7

#	Article	IF	CITATIONS
127	A Mercury surface radiometric model for SIMBIO-SYS instrument suite on board of BepiColombo mission. , 2018, , .		7
128	Characterization of the integrating sphere for the on-ground calibration of the SIMBIOSYS instrument for the BepiColombo ESA mission. Proceedings of SPIE, 2014, , .	0.8	6
129	An integrated payload design for the Atmospheric Remote-sensing Infrared Exoplanet Large-survey (ARIEL). , 2016, , .		6
130	SIMBIO-SYS/STC stereo camera calibration: Geometrical distortion. Review of Scientific Instruments, 2019, 90, 043106.	1.3	6
131	Telecentric F-theta fisheye lens for space applications. OSA Continuum, 2021, 4, 783.	1.8	6
132	QuantEYE: a quantum optics instrument for extremely large telescopes. , 2006, 6269, 635.		5
133	Stereo Camera for satellite application: A new testing method. , 2014, , .		5
134	Stray-light analyses of the METIS coronagraph on Solar Orbiter. Proceedings of SPIE, 2015, , .	0.8	5
135	Design of an afocal telescope for the ARIEL mission. Proceedings of SPIE, 2016, , .	0.8	5
136	The ARIEL ESA mission on-board metrology. , 2017, , .		5
137	Performance evaluation of the SIMBIO-SYS Stereo Imaging Channel on board BepiColombo/ESA spacecraft. Measurement: Journal of the International Measurement Confederation, 2019, 135, 828-835.	5.0	5
138	High sensitivity static Fourier transform spectrometer. Optics Express, 2021, 29, 15906.	3.4	5
139	A novel optical design for planetary surface stereo-imaging: preliminary design of the stereoscopic imaging channel of SIMBIOSYS for the BepiColombo ESA mission. , 2006, 6265, 714.		4
140	A New Stereo Algorithm based on Snakes. Photogrammetric Engineering and Remote Sensing, 2011, 77, 495-507.	0.6	4
141	Ghost images determination for the stereoscopic imaging channel of SIMBIOSYS for the BepiColombo ESA mission. Proceedings of SPIE, 2011, , .	0.8	4
142	Preliminary tolerance analysis of the coronagraphic instrument METIS for the Solar Orbiter ESA mission. , 2013, , .		4
143	The Telescope metrology Control Unit (TCU) on-board the ARIEL space mission. Measurement: Journal of the International Measurement Confederation, 2018, 122, 443-452.	5.0	4
144	Double Donut Schmidt Camera, a wide-field, large-aperture, and lightweight space telescope for the detection of ultrahigh energy cosmic rays. Applied Optics, 2018, 57, 3078.	1.8	4

#	Article	IF	CITATIONS
145	First Results of AQuEye, a Precursor â€~Quantum' Instrument for the E-ELT. Thirty Years of Astronomical Discovery With UKIRT, 2009, , 249-253.	0.3	4
146	The afocal telescope optical design and tolerance analysis for the ESA ARIEL mission. , 2017, , .		4
147	Quasi-null lens optical system for the fabrication of an oblate convex ellipsoidal mirror: application to the Wide Angle Camera of the Rosetta space mission. Applied Optics, 2006, 45, 6119.	2.1	3
148	No wavefront sensor adaptive optics system for compensation of primary aberrations by software analysis of a point source image 2 Tests. Applied Optics, 2007, 46, 6427.	2.1	3
149	Upgrade of Iqueye, a novel photon-counting photometer for the ESO New Technology Telescope. Proceedings of SPIE, 2010, , .	0.8	3
150	Coating and surface finishing definition for the Solar Orbiter/METIS inverted external occulter. , 2014, , .		3
151	DTM generation from STC-SIMBIO-SYS images. , 2015, , .		3
152	Distortion definition and correction in off-axis systems. Proceedings of SPIE, 2015, , .	0.8	3
153	Geometrical distortion calibration of the stereo camera for the BepiColombo mission to Mercury. Proceedings of SPIE, 2016, , .	0.8	3
154	A prototype for the primary mirror of the ESA ARIEL mission: design and development of an off-axis 1-m diameter aluminium mirror for infrared space applications. , 2018, , .		3
155	Qualification of the thermal stabilization, polishing and coating procedures for the aluminum telescope mirrors of the ARIEL mission. Experimental Astronomy, 2022, 53, 885-904.	3.7	3
156	<title>Optical performance of the wide-angle camera for the Rosetta mission: preliminary results</title> ., 2001, , .		2
157	Optical design of a high-spatial-resolution extreme-ultraviolet spectroheliograph for the transition region. Applied Optics, 2005, 44, 5046.	2.1	2
158	Study of the Quantum Channel between Earth and Space for Satellite Quantum Communications. Lecture Notes of the Institute for Computer Sciences, Social-Informatics and Telecommunications Engineering, 2009, , 37-40.	0.3	2
159	lqueye: a single-photon counting very high-speed photometer for the ESO 3.5m NTT. Proceedings of SPIE, 2010, , .	0.8	2
160	Alignment procedure for detector integration and characterization of the CaSSIS instrument onboard the TGO mission. , 2016, , .		2
161	Thermal architecture of the ESA ARIEL payload. , 2018, , .		2
162	The pre-launch distortion definition of SIMBIO-SYS/STC stereo camera by rational function models. , 2018, , .		2

#	Article	IF	CITATIONS
163	ESTIMATE OF DTM DEGRADATION DUE TO IMAGE COMPRESSION FOR THE STEREO CAMERA OF THE BEPICOLOMBO MISSION. International Archives of the Photogrammetry, Remote Sensing and Spatial Information Sciences - ISPRS Archives, 0, XLI-B4, 471-478.	0.2	2
164	<title>Wide-angle camera of the Rosetta mission: design and manufacturing of an innovative baffling&lt;br&gt;system for an aspherical optics telescope</title> . , 2001, , .		1
165	Observing Mercury: from Galileo to the stereo camera on the BepiColombo mission. Proceedings of the International Astronomical Union, 2010, 6, 213-218.	0.0	1
166	A method for studying the effects of thermal deformations on optical systems for space application. Proceedings of SPIE, 2010, , .	0.8	1
167	Demonstrator of the formation flying solar coronagraph ASPIICS/PROBA-3. , 2010, , .		1
168	Liquid crystals Lyot filter for solar coronagraphy. Proceedings of SPIE, 2011, , .	0.8	1
169	Determination of ghost images for the wide angle camera of the Rosetta ESA mission. Proceedings of SPIE, 2012, , .	0.8	1
170	Preliminary internal straylight analysis of the METIS instrument for the Solar Orbiter ESA mission. , 2012, , .		1
171	The CaSSIS imaging system: optical performance overview. , 2016, , .		1
172	Performances of the SIMBIO-SYS Stereo Imaging Channel (STC) on Board BepiColombo/ESA Spacecraft. , 2018, , .		1
173	Spectral response of the stereo imaging channel of SIMBIO-SYS on-board the ESA BepiColombo Mission. , 2019, , .		1
174	SIMBIOSYS-STC ready for launch: a technical recap. , 2019, , .		1
175	Study and realization of a prototype of the primary off-axis 1-m diameter aluminium mirror for the ESA ARIEL mission. , 2019, , .		1
176	The afocal telescope optical design and tolerance analysis for the ESA ARIEL Mission. , 2017, , .		1
177	A lightweight Schmidt space telescope configuration for ultra-high energy cosmic ray detection. , 2019, , .		1
178	The primary mirror of the ARIEL mission: study of thermal, figuring, and finishing treatments and optical characterization of Al 6061 samples mirrors. , 2019, , .		1
179	Calibration of the Wide-Angle Camera for the Rosetta mission: preliminary results on the flight model. , 2003, , .		0
180	Aberration estimation from single point image in a simulated adaptive optics system. , 2005, 2005, 3173-6.		0

#	Article	IF	CITATIONS
181	Effects of thermal deformations on the sensitivity of optical systems for space application. , 2010, , .		0
182	The narrow angle camera of the MPCS suite for the MarcoPolo ESA Mission: requirements and optical design solutions. Proceedings of SPIE, 2010, , .	0.8	0
183	Calibration and alignment of the demonstrator of the PROBA-3/ASPIICS formation flying coronagraph. , 2010, , .		0
184	Preliminary optical design of a polychromator for a Raman LIDAR for atmospheric calibration of the Cherenkov Telescope Array. Proceedings of SPIE, 2012, , .	0.8	0
185	Preliminary LSF and MTF determination for the stereo camera of the BepiColombo mission. Proceedings of SPIE, 2014, , .	0.8	0
186	Thin-film optical pass band filters based on new photo-lithographic process for CaSSIS FPA detector on Exomars TGO mission: development, integration, and test. Proceedings of SPIE, 2016, , .	0.8	0
187	Optical design and performance of the Stereoscopic Imaging Channel for the ESA BepiColombo mission. , 2017, , .		0
188	The afocal telescope of the ESA ARIEL mission: analysis of the layout. , 2017, , .		0
189	A novel optical design for the stereo channel of the imaging system SIMBIOSYS for the BepiColombo ESA mission. , 2017, , .		0
190	Preliminary calibration results of the wide angle camera of the imaging instrument OSIRIS for the Rosetta mission. , 2017, , .		0
191	Off-axis surface tolerance analysis: tips and tricks. , 2018, , .		0
192	Design of the instrument and telescope control units integrated subsystem of the ESA-ARIEL payload. , 2018, , .		0
193	The optical configuration of the telescope for the ARIEL ESA mission. , 2018, , .		Ο
194	Distortion calculation and removal for an off-axis and wide angle camera. , 2019, , .		0